Journal of Solid Mechanics Vol. 9, No. 1 (2017) pp. 138-156

Whirling Analysis of Axial-Loaded Multi-Step Timoshenko Rotor Carrying Concentrated Masses

K. Torabi [1,*], H. Afshari [2], H. Najafi [3]

[1]*Faculty of Mechanical Engineering, University of Isfahan, Isfahan, Iran*
[2]*Faculty of Mechanical Engineering, University of Kashan, Kashan, Iran*
[3]*Department of Solid Mechanics, Faculty of Mechanical Engineering, Politecnico di Milano, Milan, Italy*

Received 12 November 2016; accepted 14 January 2017

ABSTRACT

In this paper, exact solution for two-plane transverse vibration analysis of axial-loaded multi-step Timoshenko rotor carrying concentrated masses is presented. Each attached element is considered to have both translational and rotational inertia. Forward and backward frequencies and corresponding modes are obtained using transfer matrix method (TMM). The effect of the angular velocity of spin, value of the translational and rotational inertia, position of the attached elements and applied axial force on the natural frequencies are investigated for various boundary conditions.

Keywords : Whirling analysis; Timoshenko rotor; Multi-step; Axial load; Concentrated mass; Rotational inertia ; Transfer matrix method (TMM).

1 INTRODUCTION

THE rotor dynamics is concerned with study of dynamic and stability characteristics of the rotating machineries and plays an important role in the improving safety and performance of the entire systems that they are part of. As the rotational velocity of a rotor increases, its level of vibration often passes through critical speeds, commonly excited by unbalance of the rotating structure. If the amplitude of vibration at these critical speeds is excessive, catastrophic failure can occur. In order to achieve an optimum design and satisfy the limitations imposed by assembly considerations, stepped rotors are more used rather than uniform ones; On the other hand, existence of elements of power transmission on the rotor such as gears, pulleys and sprockets effects on the natural frequencies and critical speeds of the rotor. Each element can be modeled as a concentrated mass having translational and rotational inertias which lead to local discontinuity on the natural parameters of the rotor.

Extensive researches have been carried out with regard to the vibration analysis of the stationary beams carrying concentrated masses. Chen [1] introduced the mass by the Dirac delta function and solved analytically the problem of a vibrating simply supported beam carrying a concentrated mass at its middle section. Laura et al. [2] studied the cantilever beam carrying a lumped mass at the top, introducing the mass in the boundary conditions. Rossit and Laura [3] presented a solution for vibration analysis of a cantilever beam with a spring-mass system attached on the free end. In all of this studies, authors used Bernoulli-Euler beam theory to model simple structures, which is reliable just for slender beams. In order to increase accuracy and reliability of the studies, especially for the short structures, some authors used Timoshenko beam theory; e.g., Rao et al. [4] used coupled displacement field method to study about natural frequencies of a Timoshenko beam with a central point mass and Rossit and Laura [5] extended their previous research for Timoshenko beam theory. Laura et al. [6] considered the rotary inertia of

*Corresponding author. Tel.: +98 31 37934085; Fax: +98 31 37932746.
E-mail address: k.torabi@eng.ui.ac.ir (K.Torabi).

concentrated masses attached to the slender beams and plates and obtained fundamental frequencies of the coupled systems by means of the Rayleigh–Ritz and Dunkerley methods. Rossi and Laura [7] focused on vibrations of a Timoshenko beam clamped at one end and carrying a finite mass at the other. They considered both the translational and rotational inertia of the attached mas. Maiz et al. [8] presented an exact solution for the transverse vibration of Bernoulli–Euler beam carrying point masses and taking into account their rotary inertia. Lin [9] used numerical assembly method to determine the exact natural frequencies and mode shapes of a multi-span Timoshenko beam carrying number of various concentrated elements including point masses, rotary inertias, linear springs, rotational springs and spring–mass systems. Guitirrez et al. [10] studied stepped Timoshenko beam, elastically restrained at one end and carrying a mass having rotary inertia at the other one.

In comparison with the studies done about vibration of stationary beams, number of the studies regarding the vibration analysis of the rotors is so limit. Using finite element method, Nelson [11] studied the vibration analysis of the Timoshenko rotor with internal damping under axial load. Edney et al. [12] hired this method and proposed dynamic analysis of the tapered Timoshenko rotor. They considered viscous and hysteretic material damping, mass eccentricity and axial torque. In addition to numerical approaches, some authors focused on the analytic solutions; Zu and Han [13] proposed an exact solution for vibration analysis of the Timoshenko rotor with general boundary conditions. Jun and Kim [14] studied free bending vibration of a rotating shaft under a constant torsional torque. They modeled rotor as a Timoshenko beam and gyroscopic effect and applied torque at each part of the shaft were considered. Banerjee and Su [15] derived dynamic stiffness formulation of a composite spinning beams and studied the vibration analysis of composite rotors. The most advantage of their work was the inclusion of the bending-torsion coupling effect that arises from the ply orientation and stacking sequence in laminated fibrous composites. Hosseini and Khadem [16] studied free vibrations of an in-extensional simply supported rotating shaft with nonlinear curvature and inertia. In their research rotary inertia and gyroscopic effects are included, but shear deformation is neglected. For large amplitude vibrations, which lead to nonlinearities in curvature and inertia, Hosseini et al. [17] used method of multiple scales and investigated free vibration and primary resonances of an inextensional spinning beam with six general boundary conditions. Using differential quadrature element method (DQEM), Afshari et al. [18] presented a numerical solution for whirling analysis of multi-step multi-span Timoshenko rotors. In their work no limitation was considered in number of steps and bearings.

Transfer Matrix Method (TMM) is an exact approach for solving problems with discontinuity in domain of solution; this method is based on the changes of the vibration modes in the vicinity of the any discontinuity. Many authors used this method to solve the problems with local discontinuity. e.g. Wu and Chen [19] studied free vibration of a multi-step Timoshenko beam carrying eccentric lumped masses with rotary inertias. They also used this method and investigated free vibration analysis of a non-uniform beam with various boundary conditions and carrying multiple concentrated elements [20]. Wu and Chang [21] studied free vibration of axial-loaded multi-step Timoshenko beam carrying arbitrary concentrated elements. Khaji et al. [22] presented closed-form solutions for vibration analysis of cracked Timoshenko beams with various boundary conditions. Torabi et al. [23] studied free transverse vibration analysis of a multi-step beam carrying concentrated masses having rotary inertia for various boundary conditions. In their research both Bernoulli-Euler and Timoshenko were considered.

As mentioned, some authors studied vibration of rotors without considering effect of attached elements and some investigated these effects for stationary rotor (beam); in other words an exact solution for vibration analysis of continuous models of rotors, carrying concentrated elements is not presented. The purpose of this study is to derive a general exact solution for the vibration analysis of multiple-stepped Timoshenko rotors carrying concentrated masses at arbitrary points. For all concentrated elements both translational and rotational inertia are considered. Effect of the angular velocity of spin, position and value of translational and rotational inertias of attached masses on the frequencies of vibration will be studied for various boundary conditions.

2 GOVERNING EQUATIONS

As depicted in Fig. 1, a multi-step rotor carrying concentrated masses, under uniform axial load is considered. The attached *x*-*y*-*z* coordinates is an inertial frame and does not rotate with the rotor. By using the Timoshenko beam theory, the set of governing equations of free vibration of a bare uniform one can be stated as [24]

$$kGA\left(\frac{\partial^2 u_x}{\partial z^2}-\frac{\partial \varphi_y}{\partial z}\right)+P\frac{\partial^2 u_x}{\partial z^2}-\rho A\frac{\partial^2 u_x}{\partial t^2}=0 \tag{1a}$$

$$kGA\left(\frac{\partial^2 u_y}{\partial z^2}+\frac{\partial \varphi_x}{\partial z}\right)+P\frac{\partial^2 u_y}{\partial z^2}-\rho A\frac{\partial^2 u_y}{\partial t^2}=0 \tag{1b}$$

$$EI_x\frac{\partial^2 \varphi_x}{\partial z^2}-kGA\left(\frac{\partial u_y}{\partial z}+\varphi_x\right)-\rho I_p\Omega\frac{\partial \varphi_y}{\partial t}-\rho I_x\frac{\partial^2 \varphi_x}{\partial t^2}=0 \tag{1c}$$

$$EI_y\frac{\partial^2 \varphi_y}{\partial z^2}+kGA\left(\frac{\partial u_x}{\partial z}-\varphi_y\right)+\rho I_p\Omega\frac{\partial \varphi_x}{\partial t}-\rho I_y\frac{\partial^2 \varphi_y}{\partial t^2}=0 \tag{1d}$$

where $u_x(z,t), u_y(z,t), \varphi_x(z,t)$ and $\varphi_y(z,t)$ are components of displacement and rotation in *x* and *y* directions, respectively; Ω, ρ, E, G and *P* are angular velocity of spin, mass density, modulus of elasticity, shear modulus and applied axial load, respectively; Also, A, I_x, I_y and I_p are used for geometrical parameters respectively as cross-sectional area, moment of inertia about the *x* and *y* axis and polar moment of inertia; and k is called "shear correction factor" introduced to make up the geometry-dependent distribution of shear stress. This factor depends on the shape of the section and Poisson's ratio of material [25].

It is worth mentioning that as the *x-y-z* coordinates is a non-rotating coordinates (inertial frame), the Coriolis acceleration is not appeared in the set of governing equations. It should be also noted that in Eqs. (1a) to (1d) the components of bending moment (*M*) and shear force (*F*) are used and are defined as [24]:

$$M_x = EI_x\frac{\partial \varphi_x}{\partial z} \tag{2a}$$

$$M_y = EI_y\frac{\partial \varphi_y}{\partial z} \tag{2b}$$

$$F_x = kGA\left(\frac{\partial u_x}{\partial z}-\varphi_y\right)+P\frac{\partial u_x}{\partial z} \tag{2c}$$

$$F_y = kGA\left(\frac{\partial u_y}{\partial z}+\varphi_x\right)+P\frac{\partial u_y}{\partial z} \tag{2d}$$

Using following relation for a circular section:

$$I_p = 2I_x = 2I_y = 2I \tag{3}$$

Eqs. (1c) and (1d) can be written as:

$$EI\frac{\partial^2 \varphi_x}{\partial z^2}-kGA\left(\frac{\partial u_y}{\partial z}+\varphi_x\right)-2\rho I\Omega\frac{\partial \varphi_y}{\partial t}-\rho I\frac{\partial^2 \varphi_x}{\partial t^2}=0 \tag{4a}$$

$$EI\frac{\partial^2 \varphi_y}{\partial z^2}+kGA\left(\frac{\partial u_x}{\partial z}-\varphi_y\right)+2\rho I\Omega\frac{\partial \varphi_x}{\partial t}-\rho I\frac{\partial^2 \varphi_y}{\partial t^2}=0 \tag{4b}$$

For *m*-th segment of the rotor ($m = 1,2,3,...n+1$) (see Fig.1).

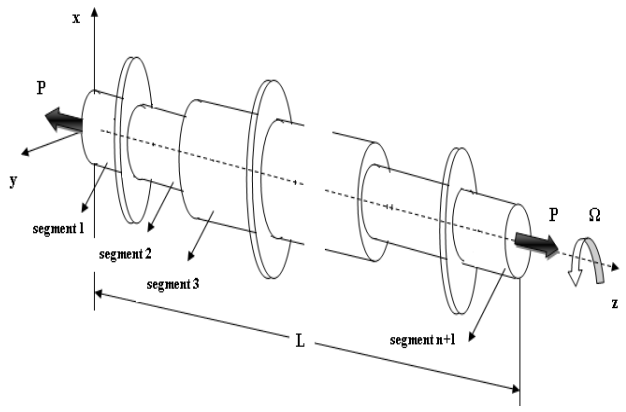

Fig.1
Multi-step rotor carrying concentrated masses, under uniform axial load.

Eqs. (1a), (1b), (4a) and (4b) can be written as:

$$kGA_m\left(\frac{\partial^2 u_x^{(m)}}{\partial z^2}-\frac{\partial \varphi_y^{(m)}}{\partial z}\right)+P\frac{\partial^2 u_x^{(m)}}{\partial z^2}-\rho A_m\frac{\partial^2 u_x^{(m)}}{\partial t^2}=0 \tag{5a}$$

$$kGA_m\left(\frac{\partial^2 u_y^{(m)}}{\partial z^2}+\frac{\partial \varphi_x^{(m)}}{\partial z}\right)+P\frac{\partial^2 u_y^{(m)}}{\partial z^2}-\rho A_m\frac{\partial^2 u_y^{(m)}}{\partial t^2}=0 \tag{5b}$$

$$EI_m\frac{\partial^2 \varphi_x^{(m)}}{\partial z^2}-kGA_m\left(\frac{\partial u_y^{(m)}}{\partial z}+\varphi_x^{(m)}\right)-2\rho I_m\Omega\frac{\partial \varphi_y^{(m)}}{\partial t}-\rho I_m\frac{\partial^2 \varphi_x^{(m)}}{\partial t^2}=0 \tag{5c}$$

$$EI_m\frac{\partial^2 \varphi_y^{(m)}}{\partial z^2}+kGA_m\left(\frac{\partial u_x^{(m)}}{\partial z}-\varphi_y^{(m)}\right)+2\rho I_m\Omega\frac{\partial \varphi_x^{(m)}}{\partial t}-\rho I_m\frac{\partial^2 \varphi_y^{(m)}}{\partial t^2}=0 \tag{5d}$$

where A_m and I_m indicate the corresponding geometrical parameter in *m*-th segment of the rotor. By introducing following complex variables $(i^2=-1)$:

$$u_m=u_x^{(m)}+iu_y^{(m)} \tag{6a}$$

$$\varphi_m=\varphi_x^{(m)}+i\,\varphi_y^{(m)} \tag{6b}$$

Eqs. (5a) to (5d) reduce to

$$kGA_m\left(\frac{\partial^2 u_m}{\partial z^2}+i\frac{\partial \varphi_m}{\partial z}\right)+P\frac{\partial^2 u_m}{\partial z^2}-\rho A_m\frac{\partial^2 u_m}{\partial t^2}=0 \tag{7a}$$

$$EI_m\frac{\partial^2 \varphi_m}{\partial z^2}+kGA_m\left(i\frac{\partial u_m}{\partial z}-\varphi_m\right)+2i\,\rho I_m\Omega\frac{\partial \varphi_m}{\partial t}-\rho I_m\frac{\partial^2 \varphi_m}{\partial t^2}=0 \tag{7b}$$

Uncoupling u_m and φ_m in Eqs. (7a) and (7b) yield the following relations:

$$\frac{\partial \varphi_m}{\partial z} = i\left[\left(1+\frac{P}{kGA_m}\right)\frac{\partial^2 u_m}{\partial z^2} - \frac{\rho}{kG}\frac{\partial^2 u_m}{\partial t^2}\right] \tag{8a}$$

$$\begin{aligned} &EI_m\left(1+\frac{P}{kGA_m}\right)\frac{\partial^4 u_m}{\partial z^4} - \rho I\left(1+\frac{E}{kG}+\frac{P}{kGA_m}\right)\frac{\partial^4 u_m}{\partial z^2 \partial t^2} + 2i\,\rho I_m \Omega\left(1+\frac{P}{kGA_m}\right)\frac{\partial^3 u_m}{\partial z^2 \partial t} \\ &-P\frac{\partial^2 u_m}{\partial z^2} + \frac{\rho^2 I_m}{kG}\frac{\partial^4 u_m}{\partial t^4} - 2i\,\frac{\rho^2 I_m \Omega}{kG}\frac{\partial^3 u_m}{\partial t^3} + \rho A_m \frac{\partial^2 u_m}{\partial t^2} = 0 \end{aligned} \tag{8b}$$

By using the method of separation of variables and introducing dimensionless spatial coordinate as:

$$\zeta = \frac{z}{L} \quad u_m(\zeta,t) = L v_m(\zeta) e^{i\omega t} \quad \varphi_m(\zeta,t) = \psi_m(\zeta) e^{i\omega t} \tag{9}$$

where ω is the circular natural frequency of whirling. Eqs. (8a) and (8b) can be written in the following dimensionless form:

$$\psi_m' = i\left(s^2\lambda^2 v_m + \frac{\kappa_m + P^*}{\kappa_m} v_m''\right) \tag{10a}$$

$$v_m^{(4)} + 2d_{1m} v_m'' + d_{2m} v_m = 0 \tag{10b}$$

where the prime indicates the derivative with respect to the dimensionless spatial variable (ζ) and the following dimensionless parameters are defined:

$$\begin{aligned} &\eta_k = \frac{d_{k+1}}{d_k} \qquad \kappa_m = \prod_{k=1}^{m-1}\eta_k^2 \qquad r^2 = \frac{I_1}{A_1 L^2} \qquad s^2 = \frac{EI_1}{kGA_1 L^2} \qquad \gamma^2 = \frac{\rho A_1 L^4 \Omega^2}{EI_1} \\ &\lambda^2 = \frac{\rho A_1 L^4 \omega^2}{EI_1} \qquad P^* = \frac{P}{kGA_1} \qquad {}_{1m} = \frac{\kappa_m^2 s^4 \lambda^2 - P^*}{2\kappa_m s^2\left(\kappa_m + P^*\right)} + \frac{r^2\lambda(\lambda-2\gamma)}{2} \qquad d_{2m} = \lambda^2\frac{\kappa_m s^2 r^2 \lambda(\lambda-2\gamma)-1}{\kappa_m + P^*} \end{aligned} \tag{11}$$

In which d_k is the diameter of the rotor at *k*-th segment. Also using Eqs. (2), (6), (9) and (11), resultant bending moment and shear force at each section of the rotor can be defined in the following form:

$$M_m = M_x + iM_y = \frac{EI_1}{L}\kappa_m^2 \psi_m' \tag{12a}$$

$$F_m = F_x + iF_y = kA_1 G\kappa_m\left(v_m' + i\psi_m + \frac{P^*}{\kappa_m} v_m'\right) \tag{12b}$$

It is worth mentioning that in a rotating beam two kind of frequencies can be found. When whirling and spin of the rotor are in the same direction $(\omega\Omega \succ 0)$, forward whirling occurs and when they are in opposite directions $(\omega\Omega \succ 0)$, backward one occurs. Solution of Eqs. (10a) and (10b) depends on the sign of d_{2m} which differs at low or high frequencies. In practice lower frequencies are more important than higher ones; thus, as d_{2m} is a negative parameter at these modes, following solution can be found:

$$v_m(\zeta) = v_0\left[A_m \cosh(\beta_{1m}\zeta) + B_m \sinh(\beta_{1m}\zeta) + C_m \cos(\beta_{2m}\zeta) + D_m \sin(\beta_{2m}\zeta)\right] \tag{13a}$$

$$\psi_m(\zeta)=iv_0\left[A_m m_{1m}\sinh(\beta_{1m}\zeta)+B_m m_{1m}\cosh(\beta_{1m}\zeta)+C_m m_{2m}\sin(\beta_{2m}\zeta)-D_m m_{2m}\cos(\beta_{2m}\zeta)\right] \quad (13b)$$

In which v_0 is a complex coefficient and

$$\begin{aligned} m_{1m}&=\frac{\beta_{1m}^2+s^2\lambda^2}{\beta_{1m}} \qquad \beta_{1m}=\sqrt{-d_{1m}+\sqrt{d_{1m}^2-d_{2m}}} \\ m_{2m}&=\frac{-\beta_{2m}^2+s^2\lambda^2}{\beta_{2m}} \qquad \beta_{2m}=\sqrt{d_{1m}+\sqrt{d_{1m}^2-d_{2m}}} \end{aligned} \quad (14)$$

3 COMPATIBILITY CONDITIONS

In the vicinity of *m*-th discontinuity, Eqs. (13a) and (13b) can be rewritten as:

$$v_m(\zeta-e_{m-1})=v_0\left\{\begin{matrix} A_m\cosh\left[\beta_{1m}(\zeta-e_{m-1})\right]+B_m\sinh\left[\beta_{1m}(\zeta-e_{m-1})\right] \\ +C_m\cos\left[\beta_{2m}(\zeta-e_{m-1})\right]+D_m\sin\left[\beta_{2m}(\zeta-e_{m-1})\right] \end{matrix}\right\} \quad (15a)$$

$$\psi_m(\zeta-e_{m-1})=iv_0\left\{\begin{matrix} A_m m_{1m}\sinh\left[\beta_{1m}(\zeta-e_{m-1})\right]+B_m m_{1m}\cosh\left[\beta_{1m}(\zeta-e_{m-1})\right] \\ +C_m m_{2m}\sin\left[\beta_{2m}(\zeta-e_{m-1})\right]-D_m m_{2m}\cos\left[\beta_{2m}(\zeta-e_{m-1})\right] \end{matrix}\right\} \quad (15b)$$

$$v_{m+1}(\zeta-e_m)=v_0\left\{\begin{matrix} A_{m+1}\cosh\left[\beta_{1(m+1)}(\zeta-e_m)\right]+B_{m+1}\sinh\left[\beta_{1(m+1)}(\zeta-e_m)\right] \\ +C_{m+1}\cos\left[\beta_{2(m+1)}(\zeta-e_m)\right]+D_{m+1}\sin\left[\beta_{2(m+1)}(\zeta-e_m)\right] \end{matrix}\right\} \quad (15c)$$

$$\psi_{m+1}(\zeta-e_m)=iv_0\left\{\begin{matrix} A_{m+1}m_{1m}\sinh\left[\beta_{1(m+1)}(\zeta-e_m)\right]+B_{m+1}m_{1(m+1)}\cosh\left[\beta_{1m}(\zeta-e_m)\right] \\ +C_{m+1}m_{2m}\sin\left[\beta_{2(m+1)}(\zeta-e_m)\right]-D_{m+1}m_{2(m+1)}\cos\left[\beta_{2m}(\zeta-e_m)\right] \end{matrix}\right\}. \quad (15d)$$

Two kind of discontinuities are considered here; stepped section and concentrated mass.

3.1 Stepped section

The compatibility conditions at a stepped section are continuity of vertical displacement, rotation, bending moment and transverse force at both *x* and *y* directions. These conditions can be modeled mathematically as:

$$\begin{aligned} &u_x^{(m)}=u_x^{(m+1)} \qquad u_y^{(m)}=u_y^{(m+1)} \qquad \varphi_x^{(m)}=\varphi_x^{(m+1)} \qquad \varphi_y^{(m)}=\varphi_y^{(m+1)} \\ &EI_m\frac{\partial\varphi_x^{(m)}}{\partial z}=EI_{m+1}\frac{\partial\varphi_x^{(m+1)}}{\partial z} \qquad EI_m\frac{\partial\varphi_y^{(m)}}{\partial z}=EI_{m+1}\frac{\partial\varphi_y^{(m+1)}}{\partial z} \\ &kGA_m\left(\frac{\partial u_x^{(m)}}{\partial z}-\varphi_y^{(m)}\right)+P\frac{\partial u_x^{(m)}}{\partial z} \qquad kGA_m\left(\frac{\partial u_y^{(m)}}{\partial z}+\varphi_x^{(m)}\right)+P\frac{\partial u_y^{(m)}}{\partial z} \\ &=kGA_{m+1}\left(\frac{\partial u_x^{(m+1)}}{\partial z}-\varphi_y^{(m+1)}\right)+P\frac{\partial u_x^{(m+1)}}{\partial z} \qquad =kGA_{m+1}\left(\frac{\partial u_y^{(m+1)}}{\partial z}+\varphi_x^{(m+1)}\right)+P\frac{\partial u_y^{(m+1)}}{\partial z} \end{aligned} \quad (16)$$

Using Eqs. (6a) and (6b), compatibility conditions reduce to

$$v_m = v_{m+1} \tag{17a}$$

$$\psi_m = \psi_{m+1} \tag{17b}$$

$$\psi'_m = \eta_m^4 \psi'_{m+1} \tag{17c}$$

$$\left(1+\frac{P^*}{\kappa_m}\right) v'_m + i\psi_m = \left(\eta_m^2 + \frac{P^*}{\kappa_m}\right) v'_{m+1} + i\eta_m^2 \psi_{m+1} \tag{17d}$$

Substituting Eqs. (15a) to (15d)into Eqs. (17a) to (17d), the constant coefficients after *m*-th discontinuity can be related on those before it as:

$$\{A_{m+1} \quad B_{m+1} \quad C_{m+1} \quad D_{m+1}\}^T = T^{(m)} \{A_m \quad B_m \quad C_m \quad D_m\}^T \tag{18}$$

where

$$T^{(m)} = \left[P^{(m)}\right]^{-1} Q^{(m)}$$

$$P^{(m)} = \begin{bmatrix} 1 & 0 & 1 & 0 \\ 0 & m_{1(m+1)} & 0 & -m_{2(m+1)} \\ m_{1(m+1)}\beta_{1(m+1)}\eta_m^4 & 0 & m_{2(m+1)}\beta_{2(m+1)}\eta_m^4 & 0 \\ 0 & \left(\eta_m^2 + \frac{P^*}{\kappa_m}\right)\beta_{1(m+1)} - \eta_m^2 m_{1(m+1)} & 0 & \left(\eta_m^2 + \frac{P^*}{\kappa_m}\right)\beta_{2(m+1)} + \eta_m^2 m_{2(m+1)} \end{bmatrix} \tag{19}$$

$$Q^{(m)} = \begin{bmatrix} \cosh(\beta_{1m}\delta_m) & \sinh(\beta_{1m}\delta_m) & \cos(\beta_{2m}\delta_m) & \sin(\beta_{2m}\delta_m) \\ m_{1m}\sinh(\beta_{1m}\delta_m) & m_{1m}\cosh(\beta_{1m}\delta_m) & m_{2m}\sin(\beta_{2m}\delta_m) & -m_{2m}\cos(\beta_{2m}\delta_m) \\ m_{1m}\beta_{1m}\cosh(\beta_{1m}\delta_m) & m_{1m}\beta_{1m}\sinh(\beta_{1m}\delta_m) & m_{2m}\beta_{2m}\cos(\beta_{2m}\delta_m) & m_{2m}\beta_{2m}\sin(\beta_{2m}\delta_m) \\ \left[\left(1+\frac{P^*}{\kappa_m}\right)\beta_{1m} \right] \sinh(\beta_{1m}\delta_m) & \left[\left(1+\frac{P^*}{\kappa_m}\right)\beta_{1m}\right]\cosh(\beta_{1m}\delta_m) & -\left[\left(1+\frac{P^*}{\kappa_m}\right)\beta_{2m}\right]\sin(\beta_{2m}\delta_m) & \left[\left(1+\frac{P^*}{\kappa_m}\right)\beta_{2m}\right]\cos(\beta_{2m}\delta_m) \\ -m_{1m} & -m_{1m} & +m_{2m} & +m_{2m} \end{bmatrix}$$

In which

$$\delta_m = e_m - e_{m-1} \tag{20}$$

3.2 Concentrated mass

The compatibility conditions at the position of an attached mass are continuity of vertical displacement and rotation and discontinuity in bending moment and transverse force at both *x* and *y* directions which can be modeled mathematically as:

$$
\begin{array}{ll}
u_x^{(m)} = u_x^{(m+1)} \qquad u_y^{(m)} = u_y^{(m+1)} \qquad \varphi_x^{(m)} = \varphi_x^{(m+1)} \qquad \varphi_y^{(m)} = \varphi_y^{(m+1)} & \\
EI_{m+1}\dfrac{\partial \varphi_x^{(m+1)}}{\partial z} - EI_m \dfrac{\partial \varphi_x^{(m)}}{\partial z} & EI_{m+1}\dfrac{\partial \varphi_y^{(m+1)}}{\partial z} - EI_m \dfrac{\partial \varphi_y^{(m)}}{\partial z} \\
= j_m \dfrac{\partial^2 \varphi_x^{(m+1)}}{\partial t^2} + 2 j_m \Omega \dfrac{\partial \varphi_y^{(m+1)}}{\partial t} & = j_m \dfrac{\partial^2 \varphi_y^{(m+1)}}{\partial t^2} - 2 j_m \Omega \dfrac{\partial \varphi_x^{(m+1)}}{\partial t} \\
kGA_m\left(\dfrac{\partial u_x^{(m+1)}}{\partial z} - \varphi_y^{(m+1)}\right) - kGA_m\left(\dfrac{\partial u_x^{(m)}}{\partial z} - \varphi_y^{(m)}\right) & kGA_m\left(\dfrac{\partial u_y^{(m+1)}}{\partial z} + \varphi_x^{(m+1)}\right) - kGA_m\left(\dfrac{\partial u_y^{(m)}}{\partial z} + \varphi_x^{(m)}\right) \\
+P\dfrac{\partial u_x^{(m+1)}}{\partial z} - P\dfrac{\partial u_x^{(m)}}{\partial z} = m_m \dfrac{\partial^2 u_x^{(m+1)}}{\partial t^2} & +P\dfrac{\partial u_y^{(m+1)}}{\partial z} - P\dfrac{\partial u_y^{(m)}}{\partial z} = m_m \dfrac{\partial^2 u_y^{(m+1)}}{\partial t^2}
\end{array}
\tag{21}
$$

where m_m and j_m are translational and rotational inertias of the *m*-th attached mass, respectively. Using Eqs. (6a) and (6b), compatibility conditions can be rewritten as:

$$v_m = v_{m+1} \tag{22a}$$

$$\psi_m = \psi_{m+1} \tag{22b}$$

$$\psi'_{m+1} + J_m \frac{\lambda(\lambda - 2\gamma)}{\kappa_m}\psi_{m+1} = \psi'_m \tag{22c}$$

$$v'_{m+1} + M_m \frac{\kappa_m s^2 \lambda^2}{\kappa_m + P^*} v_{m+1} = v'_m \tag{22d}$$

where

$$M_m = \frac{m_m}{\rho A_m L} \quad J_m = \frac{j_m}{\rho A_m L^3} = M_m c_m^2 \quad c_m^2 = \frac{j_m}{m_m L^2} \tag{23}$$

Actually c_m is the ratio of the gyration radius of the *m*-th attached mass to the length of the rotor. It is obvious that when *m*-th discontinuity is a concentrated mass one can write $m_{1m} = m_{1(m+1)}, \beta_{1m} = \beta_{1(m+1)}$ and $k_m = k_{m+1}$; now, similar to the procedure done at the previous section, substituting Eqs. (15a) to (15d) into Eqs. (22a) to (22d), Eqs. (18) and (19) can be derived again, where

$$
P^{(m)} = \begin{bmatrix}
1 & 0 & 1 & 0 \\
0 & m_{1m} & 0 & -m_{2m} \\
m_{1m}\beta_{1m} & \dfrac{J_m \lambda(\lambda - 2\gamma) m_{1m}}{\kappa_m} & m_{2m}\beta_{2m} & -\dfrac{J_m \lambda(\lambda - 2\gamma) m_{2m}}{\kappa_m} \\
\dfrac{M_m \kappa_m s^2 \lambda^2}{\kappa_m + P^*} & \beta_{1m} & \dfrac{M_m \kappa_m s^2 \lambda^2}{\kappa_m + P^*} & \beta_{2m}
\end{bmatrix}
\tag{24}
$$

$$
Q^{(m)} = \begin{bmatrix}
\cosh(\beta_{1m}\delta_m) & \sinh(\beta_{1m}\delta_m) & \cos(\beta_{2m}\delta_m) & \sin(\beta_{2m}\delta_m) \\
m_{1m}\sinh(\beta_{1m}\delta_m) & m_{1m}\cosh(\beta_{1m}\delta_m) & m_{2m}\sin(\beta_{2m}\delta_m) & -m_{2m}\cos(\beta_{2m}\delta_m) \\
m_{1m}\beta_{1m}\cosh(\beta_{1m}\delta_m) & m_{1m}\beta_{1m}\sinh(\beta_{1m}\delta_m) & m_{2m}\beta_{2m}\cos(\beta_{2m}\delta_m) & m_{2m}\beta_{2m}\sin(\beta_{2m}\delta_m) \\
\beta_{1m}\sinh(\beta_{1m}\delta_m) & \beta_{1m}\cosh(\beta_{1m}\delta_m) & -\beta_{2m}\sin(\beta_{2m}\delta_m) & \beta_{2m}\cos(\beta_{2m}\delta_m)
\end{bmatrix}
$$

4 BOUNDARY CONDITIONS

In what follows, four common boundary conditions are considered to derive frequency equation. Using Eqs. (6) and (12), mathematical model of these boundary conditions is presented in Table 1.

Boundary conditions at the right side of the rotor ($\zeta = 1$) can be written in a matrix form as:

$$\left[\Lambda\right]\left\{A_{n+1} \quad B_{n+1} \quad C_{n+1} \quad D_{n+1}\right\}^{T} = \begin{Bmatrix} 0 \\ 0 \end{Bmatrix} \tag{25}$$

Table 1
Mathematical model for external boundary conditions in Timoshenko beam theory.

Boundary conditions	Mathematical model ($\alpha = 1 - e_n$)	
Simply supported(SS)	$v_1(0) = \psi_1'(0) = 0$	$v_{n+1}(\alpha) = \psi_{n+1}'(\alpha) = 0$
Simple–Clamped(SC)	$v_1(0) = \psi_1'(0) = 0$	$v_{n+1}(\alpha) = \psi_{n+1}(\alpha) = 0$
Clamped-Clamped(CC)	$v_1(0) = \psi_1(0) = 0$	$v_{n+1}(\alpha) = \psi_{n+1}(\alpha) = 0$
Cantilever(CF)	$v_1(0) = \psi_1(0) = 0$	$\psi_{n+1}'(\alpha) = \left(1 + \frac{P^*}{\kappa_{n+1}}\right) v_{n+1}'(\alpha) + i\,\psi_{n+1}(\alpha) = 0$

In which definition of the matrix $\left[\Lambda\right]$ is presented in Table 2. for various boundary cases.

Table 2
Definition of matrix $\left[\Lambda\right]$ for various boundary conditions in Timoshenko beam theory.

	$\left[\Lambda\right]$
S	$\begin{bmatrix} \cosh\left[\beta_{1(n+1)}\alpha\right] & \sinh\left[\beta_{1(n+1)}\alpha\right] & \cos\left[\beta_{2(n+1)}\alpha\right] & \sin\left[\beta_{2(n+1)}\alpha\right] \\ m_{1(n+1)}\beta_{1(n+1)}\cosh\left[\beta_{1(n+1)}\alpha\right] & m_{1(n+1)}\beta_{1(n+1)}\sinh\left[\beta_{1(n+1)}\alpha\right] & m_{2(n+1)}\beta_{2(n+1)}\cos\left[\beta_{2(n+1)}\alpha\right] & m_{2(n+1)}\beta_{2(n+1)}\sin\left[\beta_{2(n+1)}\alpha\right] \end{bmatrix}$
C	$\begin{bmatrix} \cosh\left[\beta_{1(n+1)}\alpha\right] & \sinh\left[\beta_{1(n+1)}\alpha\right] & \cos\left[\beta_{2(n+1)}\alpha\right] & \sin\left[\beta_{2(n+1)}\alpha\right] \\ m_{1(n+1)}\sinh\left[\beta_{1(n+1)}\alpha\right] & m_{1(n+1)}\cosh\left[\beta_{1(n+1)}\alpha\right] & m_{2(n+1)}\sin\left[\beta_{2(n+1)}\alpha\right] & -m_{2(n+1)}\cos\left[\beta_{2(n+1)}\alpha\right] \end{bmatrix}$
F	$\begin{bmatrix} m_{1(n+1)}\beta_{1(n+1)}\cosh\left[\beta_{1(n+1)}\alpha\right] & \left[\left(1+\frac{P^*}{\kappa_{n+1}}\right)\beta_{1(n+1)} - m_{1(n+1)}\right]\sinh\left[\beta_{1(n+1)}\alpha\right] \\ m_{1(n+1)}\beta_{1(n+1)}\sinh\left[\beta_{1(n+1)}\alpha\right] & \left[\left(1+\frac{P^*}{\kappa_{n+1}}\right)\beta_{1(n+1)} - m_{1(n+1)}\right]\cosh\left[\beta_{1(n+1)}\alpha\right] \\ m_{2(n+1)}\beta_{2(n+1)}\cos\left[\beta_{2(n+1)}\alpha\right] & -\left[\left(1+\frac{P^*}{\kappa_{n+1}}\right)\beta_{2(n+1)} + m_{2(n+1)}\right]\sin\left[\beta_{2(n+1)}\alpha\right] \\ m_{2(n+1)}\beta_{2(n+1)}\sin\left[\beta_{2(n+1)}\alpha\right] & \left[\left(1+\frac{P^*}{\kappa_{n+1}}\right)\beta_{2(n+1)} + m_{2(n+1)}\right]\cos\left[\beta_{2(n+1)}\alpha\right] \end{bmatrix}^{T}$

By substitution of Eq. (18) into Eq. (25) for $m = n, n-1, ..., 2, 1$, next relation appears as:

$$\left[\Gamma\right]\left\{A_1 \quad B_1 \quad C_1 \quad D_1\right\}^{T} = \begin{Bmatrix} 0 \\ 0 \end{Bmatrix} \tag{26}$$

where

$$\Gamma = \Lambda T^{(n)} T^{(n-1)} \ldots T^{(2)} T^{(1)} \tag{27}$$

For the rotors which their left side ($\zeta = 0$) is simply supported, implementation of boundary conditions at this side leads to $A_1 = C_1 = 0$; therefore one can simplify Eq. (26) as:

$$\begin{bmatrix} \Gamma_{12} & \Gamma_{14} \\ \Gamma_{22} & \Gamma_{24} \end{bmatrix} \begin{Bmatrix} B_1 \\ D_1 \end{Bmatrix} = \begin{Bmatrix} 0 \\ 0 \end{Bmatrix} \tag{28}$$

and for ones which their left side is clamped following equation can be derived:

$$\begin{bmatrix} \Gamma_{11} & \Gamma_{12} & \Gamma_{13} & \Gamma_{14} \\ \Gamma_{21} & \Gamma_{22} & \Gamma_{23} & \Gamma_{24} \\ 1 & 0 & 1 & 0 \\ 0 & \mathrm{m}_{11} & 0 & -\mathrm{m}_{21} \end{bmatrix} \begin{Bmatrix} A_1 \\ B_1 \\ C_1 \\ D_1 \end{Bmatrix} = \begin{Bmatrix} 0 \\ 0 \\ 0 \\ 0 \end{Bmatrix} \tag{29}$$

5 DERIVATION OF MODE SHAPES

Using obtained frequencies and coefficients from Eqs. (28) or (29), one can evaluate eigenvectors using Eqs. (15a) to (15d) and (18) and calculate mode shapes using Heaviside function (*H*) as follow:

$$v(\zeta) = v_1(\zeta) + \sum_{i=1}^{n} \left[v_{i+1}(\zeta) - v_i(\zeta) \right] \mathrm{H}(\zeta - \zeta_i) \tag{30}$$

Finally it should be stated than each mode will be normalized as its maximum be fixed at the unity.

6 NUMERICAL RESULTS AND DISCUSSION

In this section, numerical results of the presented exact solution are presented and discussed for various cases. First, in order to validate the proposed method, consider a uniform simply supported bare Timoshenko rotor ($r = 0.03,\ s = 0.05,\ P^* = 0$). Table 3. shows the value of the first four forward and backward frequencies for various values of the angular velocity of spin. Results of this table are compared with the exact results which can be easily derived using sinusoidal modes as [24]

$$\lambda^4 - 2i\gamma\lambda^3 + \frac{1 + \left(r^2 + s^2\right) n^2 \pi^2}{r^2 s^2} \lambda^2 - 2i\gamma \frac{n^2 \pi^2}{s^2} \lambda + \frac{n^4 \pi^4}{r^2 s^2} = 0 \tag{31}$$

where *n* is mode number. As this table confirms, results with high accuracies can be obtained.

In order to validate the proposed solution for beams carrying concentrated masses, consider a cantilever stationary beam ($\gamma = 0$) with a tip mass and properties which have been mentioned by Rossi and Laura, 1990. Table 4. shows value of the first three frequencies for various amounts of mass and rotary inertia. Comparison of the results confirms the high accuracy of presented solution.

After validation of the proposed solution, effect of the various parameters on the frequencies can be investigated for all the boundary conditions. In what follows, all results are derived for a Timoshenko rotor with dimensionless parameters as $r = 0.03$ and $s = 0.05$.

Table 3

Value of the first four forward and backward frequencies of a uniform simply supported bare rotor $(r = 0.03, s = 0.05, P^* = 0)$ for various values of the angular velocity of spin.

γ	Present				Genta [24]			
	Forward whirling							
	λ_1	λ_2	λ_3	λ_4	λ_1	λ_2	λ_3	λ_4
0	9.7085	37.1165	78.2528	128.9417	9.7091	37.1197	78.2611	128.9580
0.5	9.7122	37.1305	78.2788	128.9855	9.7133	37.13354	78.2870	128.9938
1	9.7170	37.1476	78.3093	129.0215	9.7175	37.1484	78.3130	129.0296
3	9.7341	37.2050	78.4149	129.1653	9.7343	37.2060	78.4168	129.1727
5	9.7500	37.2593	78.5110	129.3143	9.7511	37.2636	78.5207	129.3159
γ	Backward whirling							
	λ_1	λ_2	λ_3	λ_4	λ_1	λ_2	λ_3	λ_4
0	9.7085	37.1165	78.2528	128.9417	9.7091	37.1197	78.2611	128.9580
0.5	9.7048	37.1012	78.2299	128.9074	9.7049	37.1053	78.2351	128.9221
1	9.6700	37.0890	78.2018	128.8848	9.7007	37.0909	78.2091	128.8863
3	9.6829	37.0292	78.1024	128.7356	9.6839	37.0335	78.1053	128.7431
5	9.6670	36.9761	77.9934	128.5917	9.6672	36.9761	78.0016	128.5997

Table 4

Values of the first three frequencies of a cantilever beam with a tip mass.

	c	$M = 0.2$			$M = 0.4$		
present	0	2.5666	16.1755	41.6629	2.1343	15.3349	40.6289
Rossi & Laura [7]		2.567	16.177	41.673	2.135	15.335	40.632
Present	0.1	2.5556	15.4376	37.7985	2.1208	14.1701	34.0834
Rossi & Laura [7]		2.556	15.438	37.804	2.121	14.172	34.094

As depicted in Fig. 2 a simple-clamped stepped rotor under tension $(P^* = 0.01)$ with two same concentrated masses $(M = 0.1, c^2 = 0.05)$ is considered. For first four modes, Campbell diagram is depicted in Figs. 3(a) to 3(d). As shown in this figures, for a non-rotating rotor, value of the forward and backward frequencies are equal; but because of gyroscopic effect, as value of the velocity of spin increases, forward frequencies increase and backward ones decrease. This figures also shows the line of synchronous whirling $(\lambda = \pm\gamma)$; Intersection of this line with the Campbell diagram determines the critical speeds of the rotor which should be avoided. This diagrams also shows that as value of the velocity of spin increases, for all frequencies, backward mode is excited before corresponding forward one.

In order to investigate the influence of the gyroscopic effect on mode shapes, for the previous example, corresponding mode shapes are depicted in Figs. 4(a) to 4(d) for $\gamma = 0$ and $\gamma = 20$. As these figures shows, for a stationary rotor forward and backward modes are same but for a rotating one there is difference between forward and backward modes especially for higher modes.

Now consider two uniform rotors $(\gamma = 15, P^* = 0.05)$; a simply supported (SS) rotor with a concentrated mass located at $\zeta = 0.3$ and a simple-clamped (SC) one with a concentrated mass located at the middle section. By neglecting the rotatory inertia of the attached mass, the effect of the its translational inertia on the first five forward and backward frequencies are depicted in Figs. 5(a) to 5(d). It should be noted that in this figures, in order to be able to show all frequencies simultaneously, each frequency is divided to the corresponding value of a uniform one without any attachment (λ_0), in other words $\tau_i = \lambda_i / \lambda_{0i}$. As shown in these figures, when value of translational inertia increases, all frequencies decrease. In other words as the value of the mass of an attached element is more considerable in comparison with total mass of the rotor, there is more decrease in both forward and backward frequencies. It can be explained by increasing the inertia of the system. It is worth mentioning that amount of the decrease on each frequency is strongly dependent on the position of the attached mass which will be discussed separately later.

In addition to mass of a concentrated element, distribution of its mass around the rotation axis of rotor (axis in Fig. 1) has a significant effect on the dynamic characteristics of the rotor. As concentration of the mass locates a greater radius, value of the rotational inertia of the attached element increases. Effect of the translational inertia was

investigated in Figs. 5(a) to 5(d); As shown, it causes to decrease in all frequencies; According to Eq. (22d), this decrease is independent from angular velocity of spin; but Eq. (22c) shows that the effect of rotational inertia is dependent on the angular velocity of spin. To study this topic, consider a uniform clamped-clamped rotor under tension ($P^* = 0.05$) with a concentrated mass ($M = 0.1$) located at $\zeta = 0.4$; Figs. 6(a) to 6(h) show the effect of the rotational inertia on the first four forward and backward frequencies for various values of the velocity of spin. As shown in these figures, rotational inertia may decrease or increase a frequency; Like the translational inertia, rotational inertia increases the inertia of the system which leads to decrease in both forward and backward frequencies; but by growing rotational inertia, gyroscopic effect increases and as shown in Campbell diagram (Figs. 3(a) to 3(d)), it leads to increase in forward frequencies and decrease in backward ones. Therefore, as value of the rotational inertia increases (e.g. increasing in radius or thickness of a mounted gear on rotor), all backward frequencies decrease but forward ones may decrease or increase; according to Eq. (22c) it depends on the sign of $\lambda - 2\gamma$; In other words for low values of velocity of spin especially at high modes, rotational inertia decreases the forward frequencies and for higher values of velocity of spin especially at low modes, rotational inertia increases forward frequencies.

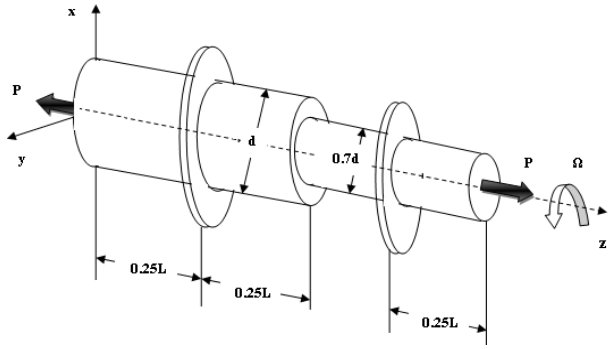

Fig.2
A simple-clamped stepped rotor under tension ($P^* = 0.01$) with two same concentrated masses ($M = 0.1, c^2 = 0.05$).

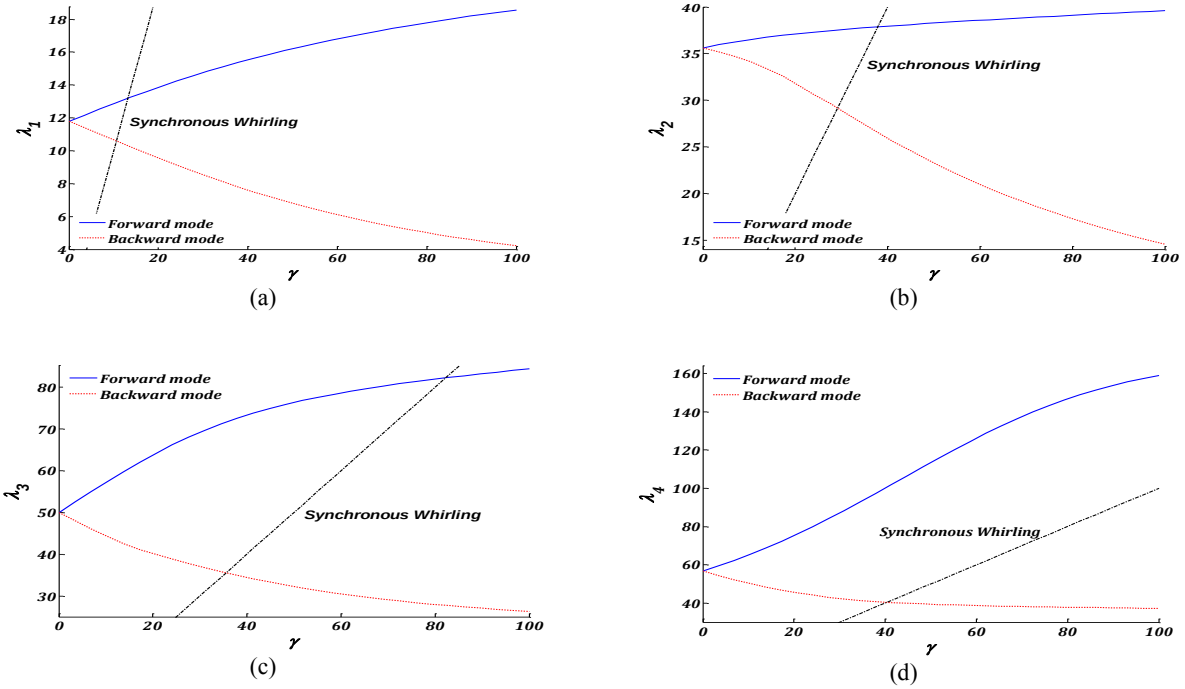

Fig.3
Campbell diagram for first four modes of the rotor depicted in Fig. 2.

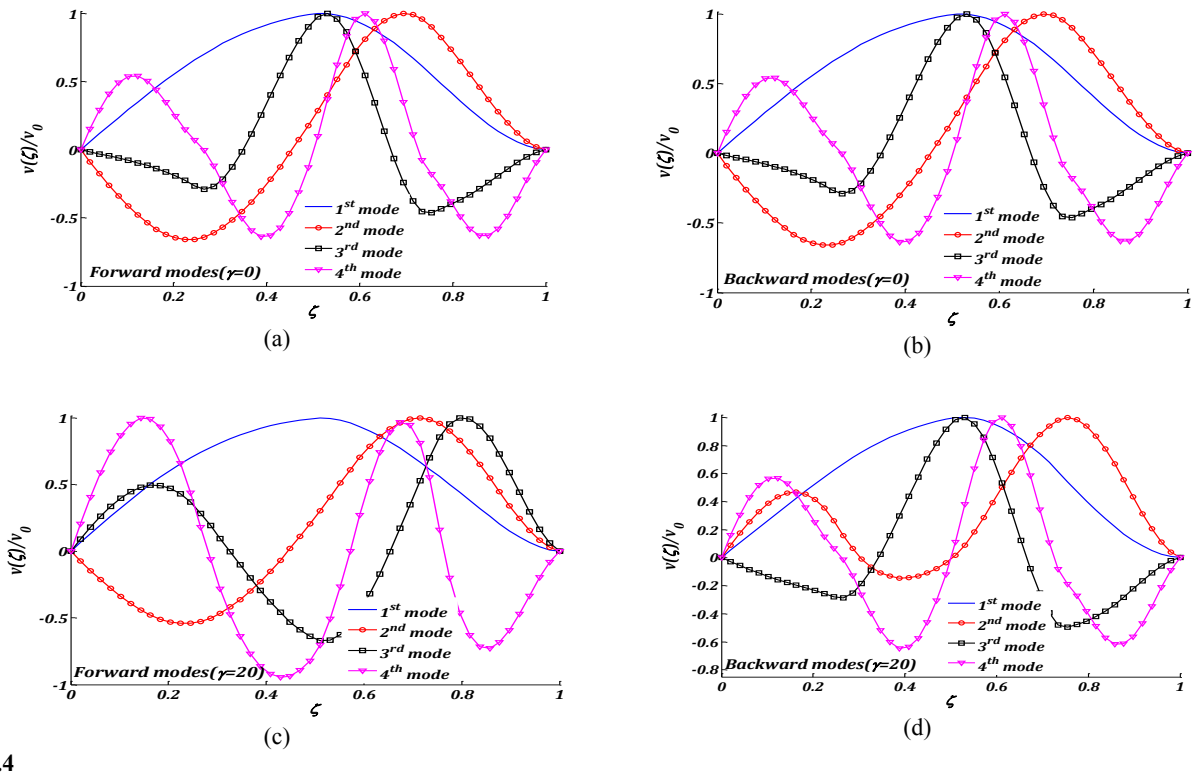

Fig.4
First four forward and backward mode shapes of the rotor depicted in Fig.2 for $\gamma = 0$ and $\gamma = 20$.

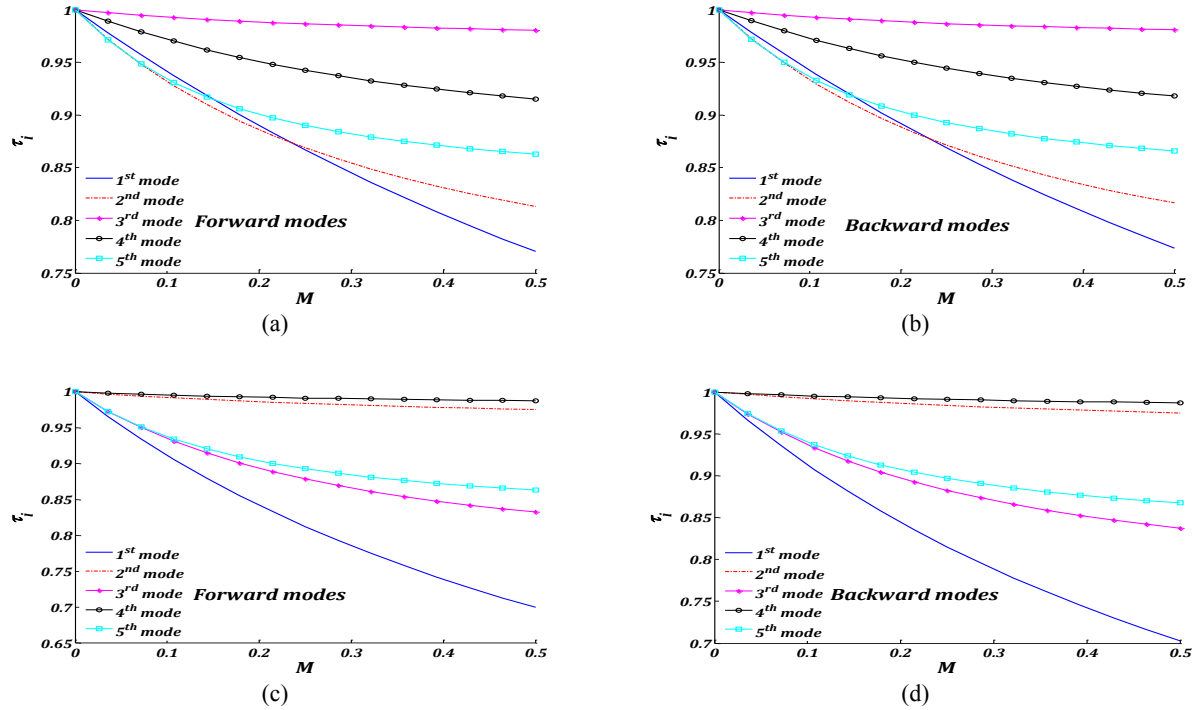

Fig.5
Effect of the translational inertia of the attached mass on the first five forward and backward frequencies of uniform rotors $(\gamma = 15, P^* = 0.05)$; a simply supported (SS) rotor with a concentrated mass located at $\zeta = 0.3$ and a simple-clamped (SC) one with a concentrated mass located at the middle section.

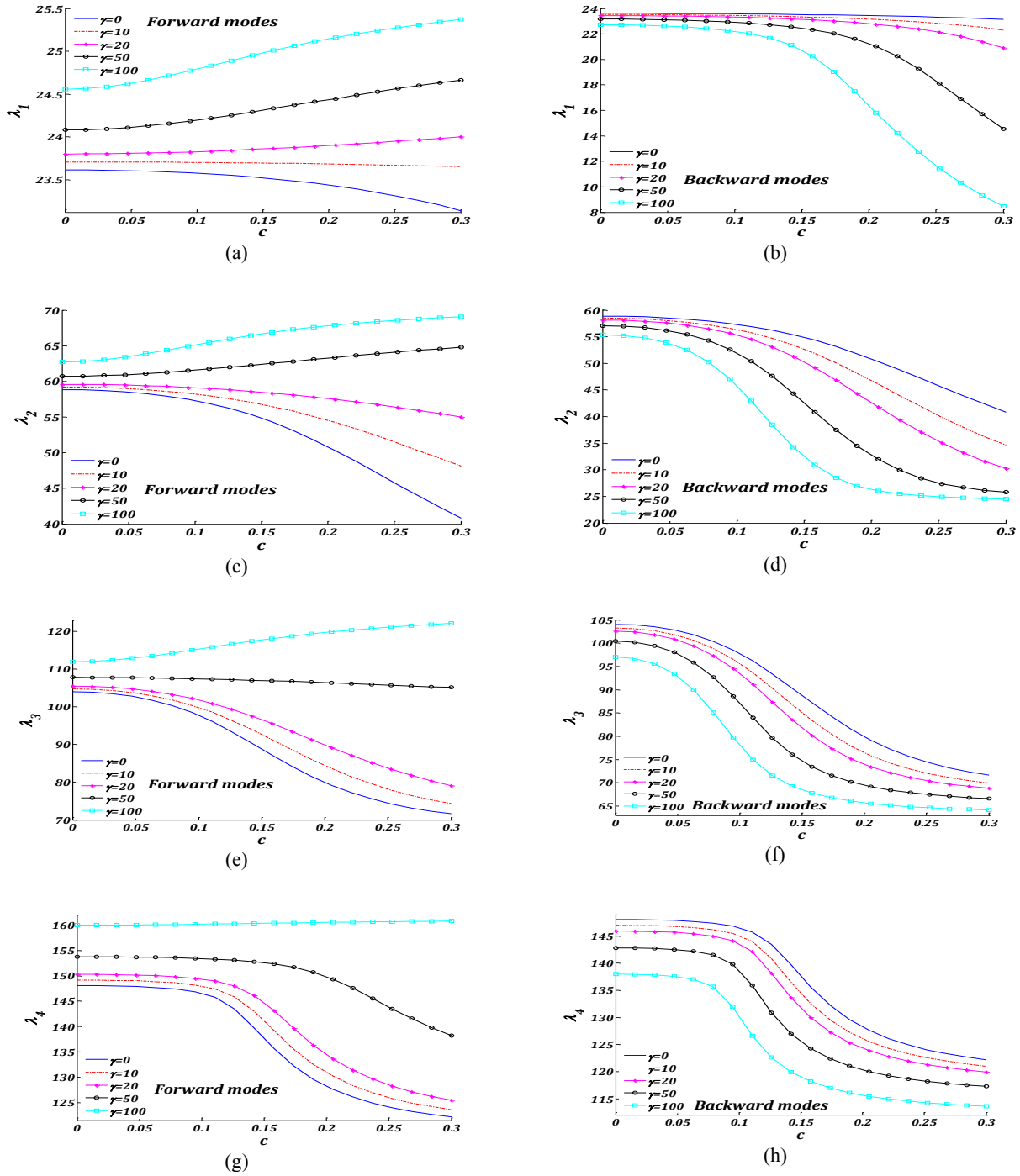

Fig.6

Variation of the first four forward and backward frequencies of a uniform clamped-clamped rotor under tension ($P^* = 0.05$) with a concentrated mass $(M = 0.1)$ located at $\zeta = 0.4$ versus variation of the rotational inertia of the attached mass for various values of velocity of spin.

Two uniform rotors $(\gamma = 5, P^* = 0.05)$ carrying a concentrated mass $(M = 0.05)$ with various values of rotational inertia with two boundary conditions is considered; a cantilever (CF) rotor and a simply supported (SS) one. Figs. 7(a) to 7(l) show the variation of the first three forward and backward frequencies versus the position of the concentrated mass for various values of rotational inertia. These figures show that in each mode, there are some

positions that when mass is located on them, there is no change in the frequencies for $c=0$; In other words, when mass located at these points, all change in corresponding frequency is affected by rotary inertia whereas translational inertia has no effect on corresponding frequency. These points are the nodes in corresponding mode, e.g. center point for even frequencies of a symmetric beam. On the other hand, there are some points that when the mass is located on them, value of change in frequency is independent from rotary inertia. In other words, when the mass located at these points, all decreases in corresponding frequency is affected by translational inertia whereas rotary inertia has no effect on the corresponding frequency. These points are antinodes of corresponding mode shape, e.g. center point for odd frequencies of a symmetric beam. As shown, number of node and antinode points increases at higher modes.

Finally the effect of the axial force on the frequencies should be investigated. Axial forces can be generated by several types of gears or thermal effects. As depicted in Fig. 8, a stepped rotor $(\gamma=20)$ with a concentrated mass $(M=0.1, c^2=0.05)$ is considered with two boundary conditions; a simply supported (SS) and a simple-clamped (SC). Figs. 9(a) to 9(d) show the effect of the axial force on the first four forward and backward frequencies. As shown in these figures, tension load increases all forward and backward frequencies whereas compressive one decreases all forward and backward frequencies to the extent of buckling of the rotor. Also, for $P^*=0.1$, corresponding mode shapes are depicted in Figs. 10(a) to 10(d).

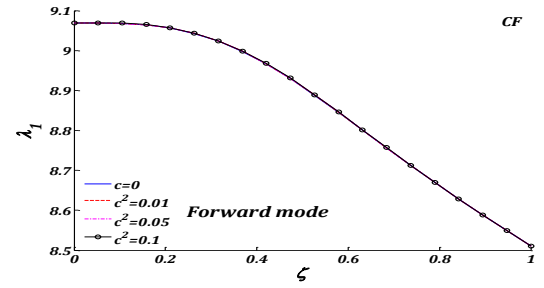

(a)

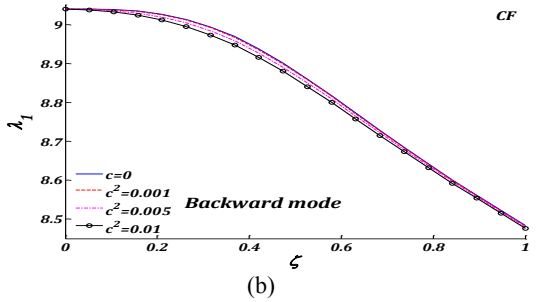

(b)

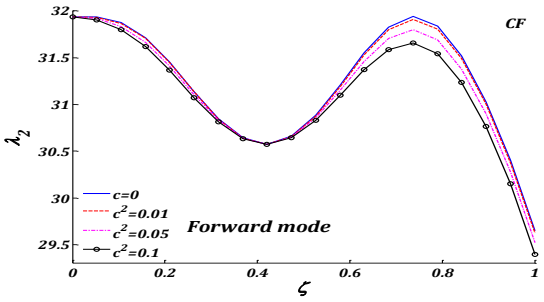

(c)

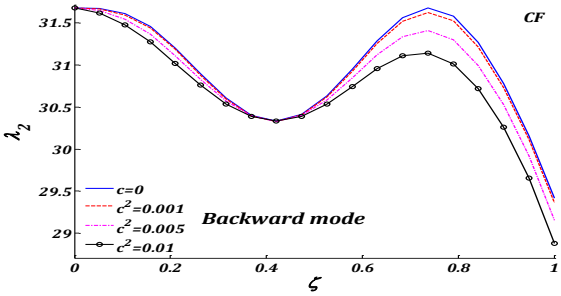

(d)

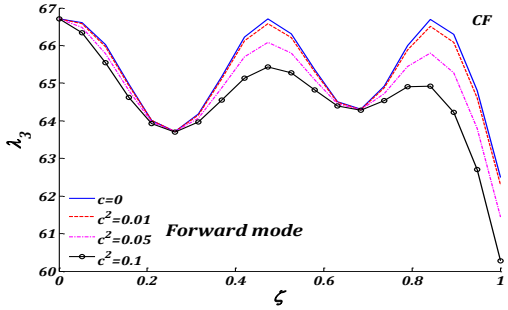

(e)

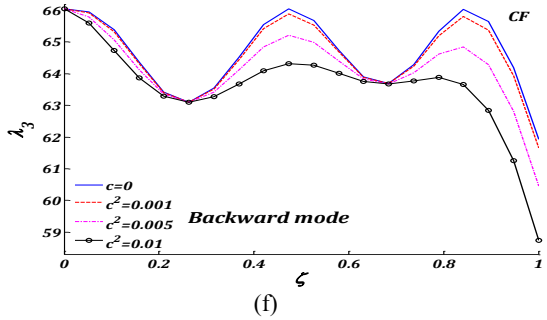

(f)

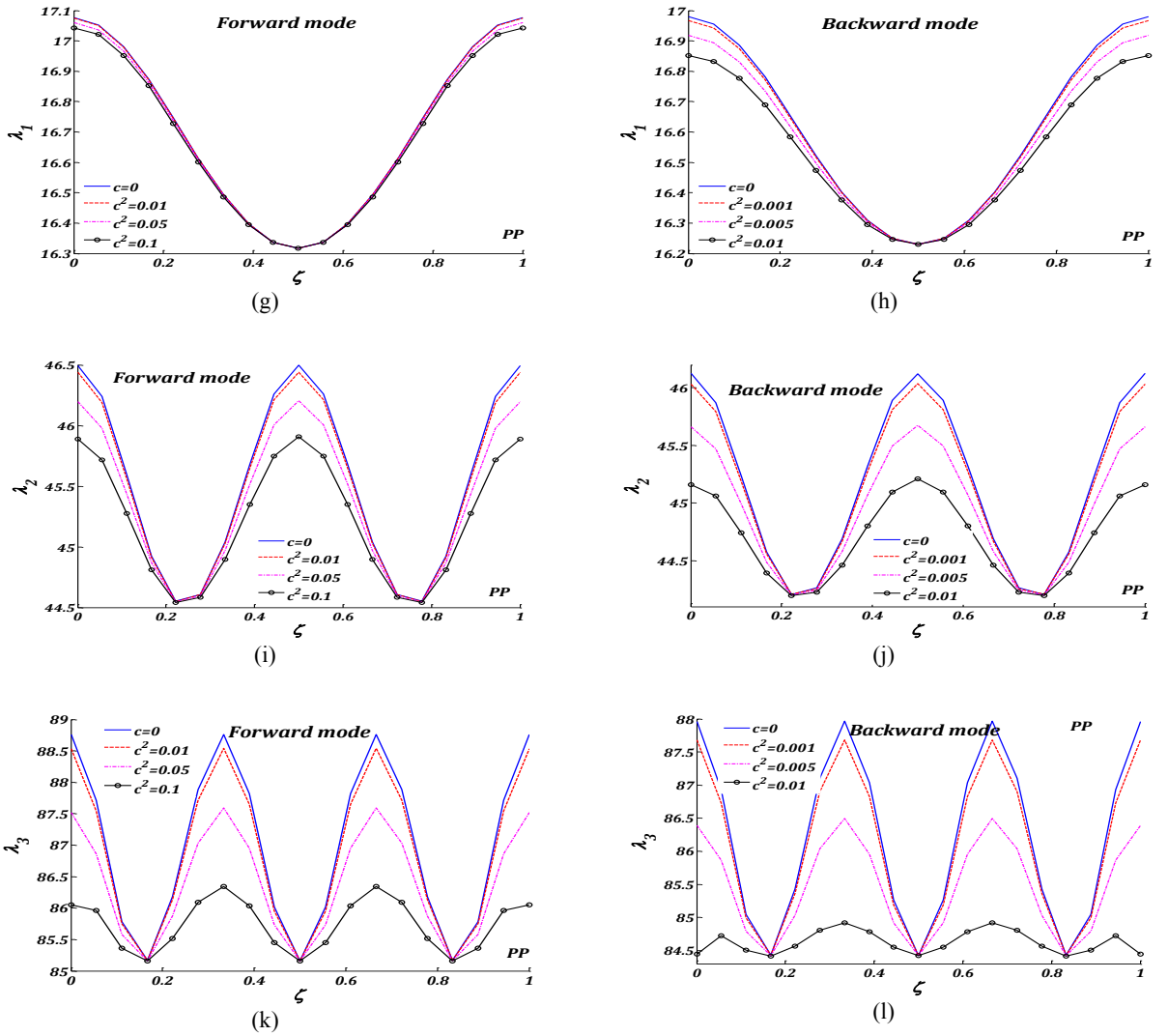

Fig.7

First three frequencies versus position of mass for variable values of rotary inertia, for two uniform rotors $(\gamma = 5, P^* = 0.05)$ carrying a concentrated mass $(M = 0.05)$; a cantilever (CF) rotor and a simply supported (SS) one.

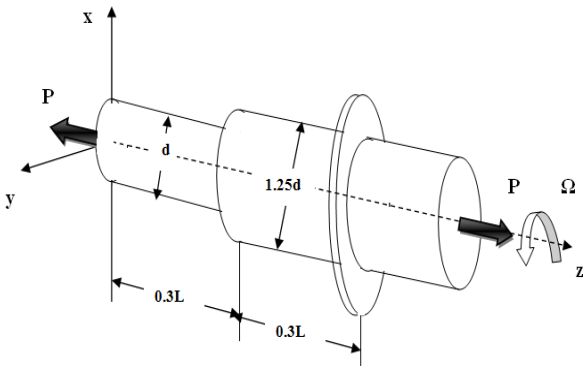

Fig.8

A stepped rotor with a concentrated mass.

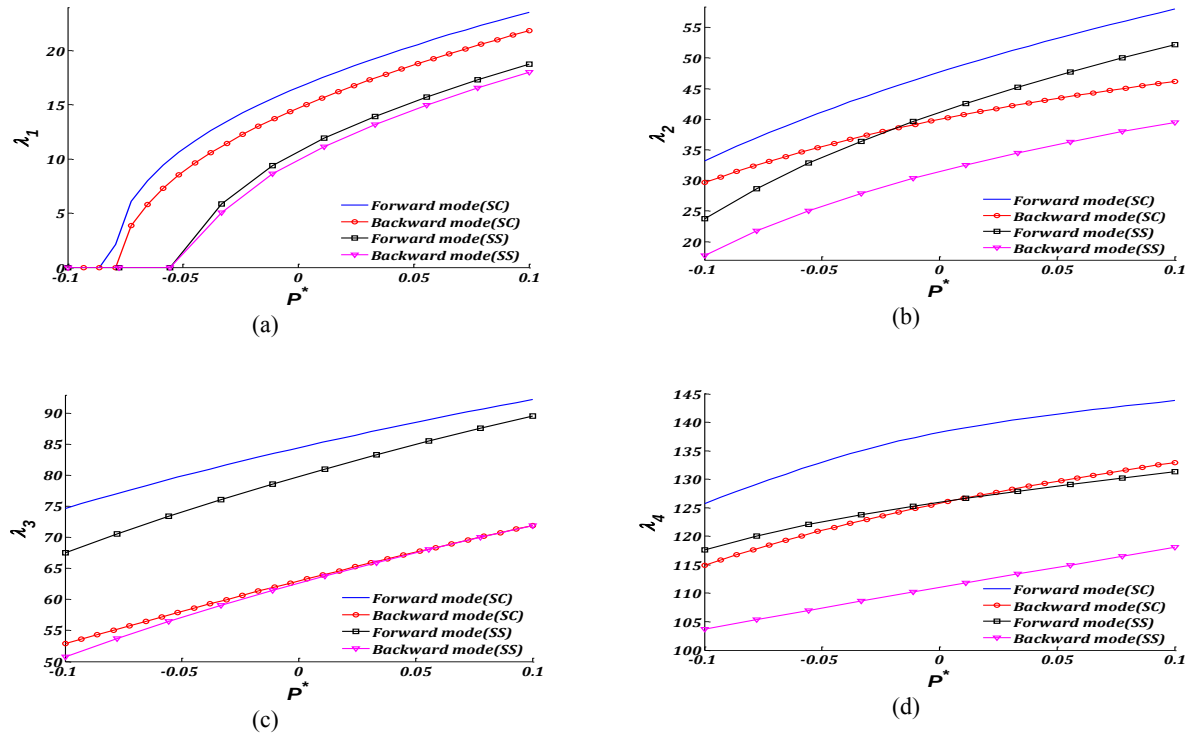

Fig.9

Effect of the axial force on the forward and backward frequencies of a stepped rotor $(\gamma = 20)$ with a concentrated mass $(M = 0.1, c^2 = 0.05)$ with two boundary conditions; a simply supported (SS) and a simple-clamped (SC).

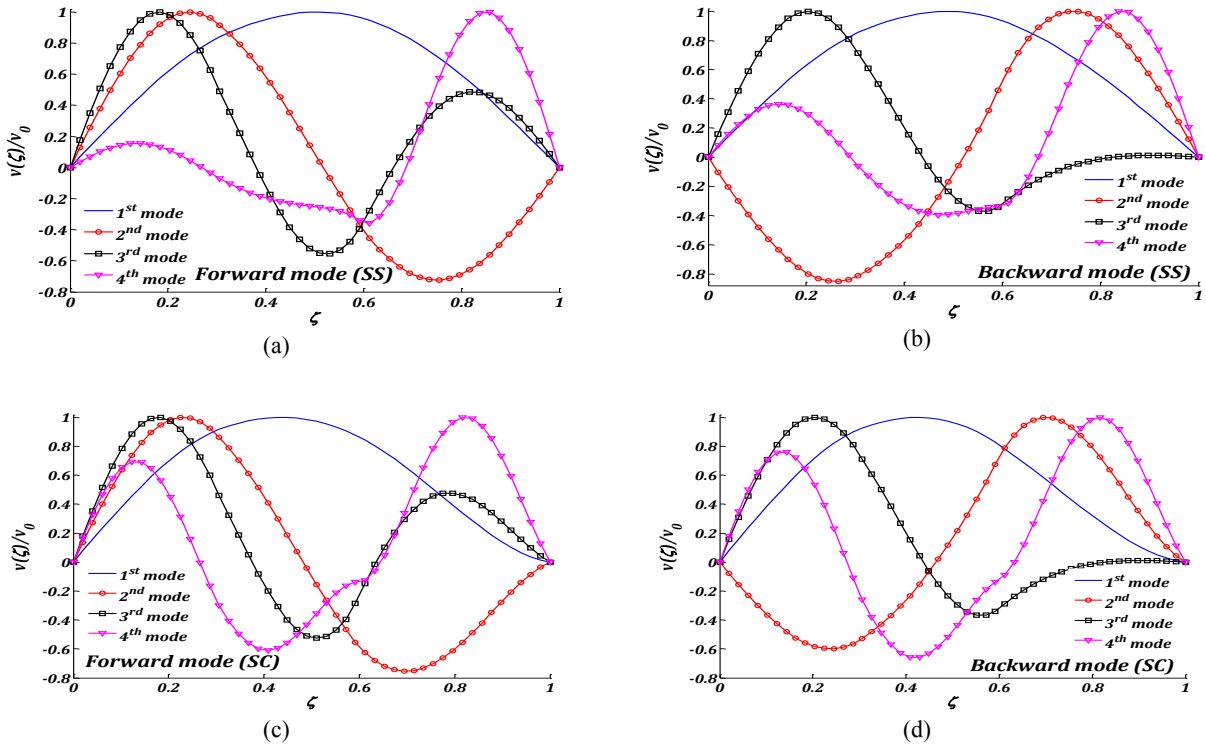

Fig.10

First four forward and backward mode shapes of the rotor depicted in Figure 8 for $P^* = 0.1$.

7 CONCLUSIONS

Using transfer matrix method, whirling analysis of multi-step Timoshenko rotor carrying concentrated masses, under axial load was presented analytically. Effect of the angular velocity of spin, translational and rotational inertias and position of the attached elements and applied axial force on the forward and backward frequencies of multi-step rotors were investigated for various boundary conditions. Summary of the results obtained from numerical examples can be listed as follows:

- For a non-rotating rotor, value of the forward and backward frequencies are equal; but because of gyroscopic effect, as value of the velocity of spin increases, forward frequencies increase and backward ones decrease.
- As value of translational inertia of the attached masses increases, all frequencies decrease; but it cannot be concluded for rotational inertia; it was shown that as value of the rotational inertia of the attached masses increases, all backward frequencies decrease but, dependent on the sign of λ-2γ, forward ones may decrease or increase.
- For each mode, there are some positions that when a mass is located on them, all change in the corresponding frequency is affected by rotary inertia; these points are the nodes in the corresponding mode. On the other hand, there are some positions that when a mass is located on them, all decreases in corresponding frequency is affected by translational inertia; these points are antinodes of the corresponding mode shape.
- Tension load increases all forward and backward frequencies whereas compressive one decreases them to the extent of buckling of the rotor.

ACKNOWLEDGEMENTS

The authors are grateful to the University of Kashan for supporting this work by Grant No. 363463/1.

REFERENCES

[1] Chen Y., 1963, On the vibration of beams or rods carrying a concentrated mass, *Journal of Applied Mechanics* **30**: 310-311.

[2] Laura P., Maurizi M.J., Pombo J.L., 1975, A note on the dynamics analysis of an elastically restrained-free beam with a mass at the free end, *Journal of Sound and Vibration* **41**: 397-405.

[3] Rossit C.A., Laura P., 2001, Transverse vibrations of a cantilever beam with a spring mass system attached on the free end, *Ocean Engineering* **28**: 933-939.

[4] Rao G.V., Saheb K.M., Janardhan G.R., 2006, Fundamental frequency for large amplitude vibrations of uniform Timoshenko beams with central point concentrated mass using coupled displacement field method, *Journal of Sound and Vibration* **298**: 221-232.

[5] Rossit C.A., Laura P., 2001, Transverse normal modes of vibration of a cantilever Timoshenko beam with a mass elastically mounted at the free end, *Journal of the Acoustical Society of America* **110**: 2837-2840.

[6] Laura P., Filipich C.P., Cortinez V.H., 1987, Vibrations of beams and plates carrying concentrated masses, *Journal of Sound and Vibration* **117**: 459-465.

[7] Rossi R.E., Laura P., 1990, Vibrations of a Timoshenko beam clamped at one end and carrying a finite mass at the other, *Applied Acoustics* **30**: 293-301.

[8] Maiz S., Bambill D., Rossit C., Laura P., 2007, Transverse vibration of Bernoulli–Euler beams carrying point masses and taking into account their rotary inertia, *Journal of Sound and Vibration* **303**: 895-908.

[9] Lin H.Y., 2009, On the natural frequencies and mode shapes of a multi-span Timoshenko beam carrying a number of various concentrated elements, *Journal of Sound and Vibration* **319**: 593-605.

[10] Gutierrez R.H., Laura P., Rossi R.E., 1991, Vibrations of a Timoshenko beam of non-uniform cross-section elastically restrained at one end and carrying a finite mass at the other, *Ocean Engineering* **18**: 129-145.

[11] Nelson H.D., 1980, A finite rotating shaft element using Timoshenko beam theory, *Journal of Mechanical Design* **102**: 793-803.

[12] Edney S.L., Fox C.H.J., Williams E.J., 1990, Tapered Timoshenko finite elements for rotor dynamics analysis, *Journal of Sound and Vibration* **137**: 463-481.

[13] Zu J.W.Z., Han R.P.S., 1992, Natural frequencies and normal modes of a spinning Timoshenko beam with general boundary conditions, *Journal of Applied Mechanics* **59**: 197-204.

[14] Jun O.S., Kim J.O., 1999, Free bending vibration of a multi-step rotor, *Journal of Sound and Vibration* **224**: 625-642.

[15] Banerjee J.R., Su H., 2006, Dynamic stiffness formulation and free vibration of a spinning composite beam, *Computers & Structures* **84**: 1208-1214.
[16] Hosseini S.A.A., Khadem S.E., 2009, Free vibrations analysis of a rotating shaft with nonlinearities in curvature and inertia, *Mechanism and Machine Theory* **44**: 272-288.
[17] Hosseini S.A.A., Zamanian M., Shams Sh., Shooshtari A., 2014, Vibration analysis of geometrically nonlinear spinning beams, *Mechanism and Machine Theory* **78**: 15-35.
[18] Afshari H., Irani M., Torabi K., 2014, Free whirling analysis of multi-step Timoshenko rotor with multiple bearing using DQEM, *Modares Mechanical Engineering* **14**: 109-120.
[19] Wu J.S., Chen C.T., 2007, A lumped-mass TMM for free vibration analysis of a multi-step Timoshenko beam carrying eccentric lumped masses with rotary inertias, *Journal of Sound and Vibration* **301**: 878-897.
[20] Wu J.S., Chen C.T., 2008, A continuous-mass TMM for free vibration analysis of a non-uniform beam with various boundary conditions and carrying multiple concentrated elements, *Journal of Sound and Vibration* **311**: 1420-1430.
[21] Wu J.S., Chang B.H., 2013, Free vibration of axial-loaded multi-step Timoshenko beam carrying arbitrary concentrated elements using continuous-mass transfer matrix method, *European Journal of Mechanics - A/Solids* **38**: 20-37.
[22] Khaji N., Shafiei M., Jalalpour M., 2009, Closed-form solutions for crack detection problem of Timoshenko beams with various boundary conditions, *International Journal of Mechanical Sciences* **51**: 667-681.
[23] Torabi K., Afshari H., Najafi H., 2013, Exact solution for free vibration analysis of multi-step Bernoulli-Euler and Timoshenko beams carrying multiple attached masses and taking into account their rotary inertia, *Journal of Solid Mechanics* **5**: 336-349.
[24] Genta G., 2005, *Dynamics of Rotating Systems*, Springer, New York.
[25] Hutchinson J.R., 2001, Shear coefficients for Timoshenko beam theory, *Journal of Applied Mechanics* **68**: 87-92.